Deciphering the rules governing assembly order of mammalian septin complexes

Mikael E. Sellin[a], Linda Sandblad[b], Sonja Stenmark[a], and Martin Gullberg[a]
[a]Department of Molecular Biology, Umeå University, SE-901 87 Umeå, Sweden; [b]Department of Cell and Molecular Biology, Karolinska Institute, S-171 77 Stockholm, Sweden

ABSTRACT **Septins are conserved GTP-binding proteins that assemble into lateral diffusion barriers and molecular scaffolds. Vertebrate genomes contain 9–17 septin genes that encode both ubiquitous and tissue-specific septins. Expressed septins may assemble in various combinations through both heterotypic and homotypic G-domain interactions. However, little is known regarding assembly states of mammalian septins and mechanisms directing ordered assembly of individual septins into heteromeric units, which is the focus of this study. Our analysis of the septin system in cells lacking or overexpressing selected septins reveals interdependencies coinciding with previously described homology subgroups. Hydrodynamic and single-particle data show that individual septins exist solely in the context of stable six- to eight-subunit core heteromers, all of which contain SEPT2 and SEPT6 subgroup members and SEPT7, while heteromers comprising more than six subunits also contain SEPT9. The combined data suggest a generic model for how the temporal order of septin assembly is homology subgroup-directed, which in turn determines the subunit arrangement of native heteromers. Because mammalian cells normally express multiple members and/or isoforms of some septin subgroups, our data also suggest that only a minor fraction of native heteromers are arranged as perfect palindromes.**

Monitoring Editor
Douglas R. Kellogg
University of California, Santa Cruz

Received: Mar 25, 2011
Revised: Jun 14, 2011
Accepted: Jun 28, 2011

INTRODUCTION

Septins comprise a family of ubiquitous GTP-binding proteins in fungi and animal cells that form heterooligomers that further assemble into an array of higher-order structures. Because septins can self-assemble and can associate with F-actin, microtubules, and membranes, they have been considered as components of the cytoskeleton (reviewed in Weirich *et al.*, 2008). In budding yeast, septins serve as a lateral diffusion barrier that restricts exchange of membrane proteins between mother and daughter bud (reviewed in Caudron and Barral, 2009) and as scaffolds that tether proteins to the bud neck (reviewed in Oh and Bi, 2011).

The main feature of septins is a conserved central GTP-binding domain (termed G-domain), which is flanked by variable N- and C-termini. Vertebrate genomes analyzed so far contain 9–17 septin genes (Cao *et al.*, 2007), and humans have 13 functional septin genes, namely *SEPT1* to *SEPT12*, and *SEPT14* (note that the former *SEPT13* is a pseudogene, *SEPT7P2*, HGNC:32339). Many of the gene products are ubiquitous, while a subset appears cell type–restricted (Hall *et al.*, 2005; Cao *et al.*, 2007). Cross-kingdom comparisons have been confounded by the evidence that animal septins fall into independent evolutionary groups (Kinoshita, 2003b). A comprehensive phylogenetic analysis has provided support for classification into five groups, of which vertebrate septins are all included in either group 1 or 2 (Pan *et al.*, 2007). Even so, based on amino acid sequence similarity, vertebrate septins can be divided into four distinct subgroups, which are named after the SEPT2, SEPT3, SEPT6, and SEPT7 founding members (Kinoshita, 2003a). Each one of these four subgroups is represented in vertebrates as well as other chordates (Cao *et al.*, 2007). However, only two or three subgroups are represented in invertebrate animal model systems, such as *Caenorhabditis elegans* and *Drosophila*. In addition, phylogenetic analysis indicates that the homology-based subgroup

This article was published online ahead of print in MBoC in Press (http://www.molbiolcell.org/cgi/doi/10.1091/mbc.E11-03-0253) on July 14, 2011.

Address correspondence to: Mikael E. Sellin (mikael.sellin@molbiol.umu.se).

Abbreviations used: EGTA, ethylene glycol tetraacetic acid; G-domain, GTP-binding domain; qRT-PCR, quantitative real-time PCR; SEPT6-Flag, SEPT6 derivative with an eight-amino-acid FLAG; shRNA, short hairpin RNA.

classification of vertebrate septins is not informative with respect to orthologous relationships between animal and fungal septins (Cao *et al.*, 2007). Thus, the functional significance of current classification systems remains unclear, hampering comparisons between yeast and animal model systems, as well as between vertebrates and invertebrates.

As shown by electron microscopy, septins can form stable rod-shaped oligomeric complexes that assemble into filaments by end-to-end association and lateral interactions under conditions of low ionic strength. Analyses of native and recombinant complexes have revealed tetrameric, hexameric, or octameric heteromer units, depending on the source organism (Field *et al.*, 1996; John *et al.*, 2007; Sirajuddin *et al.*, 2007; Bertin *et al.*, 2008; Lukoyanova *et al.*, 2008). The septin family members are arranged in a nonrandom order within heteromeric units (Weirich *et al.*, 2008). However, overexpression of single or multiple septins in animal cells results in various types of homo- and heteromeric structures, as well as insoluble filaments and aggregates that, at least in part, may represent nonphysiological assembly states (reviewed in Kinoshita, 2003a).

A recent structural study was based on the findings that 1) recombinant expression of SEPT2 yields dimers that polymerize into filaments and 2) bacterial coexpression of human SEPT2, SEPT6, and SEPT7 yields uniformly sized heteromers of a defined composition (Mendoza *et al.*, 2002; Sheffield *et al.*, 2003). Crystal structures of the bacterially expressed septins revealed two types of interfaces residing on opposite sides of the G-domain (Sirajuddin *et al.*, 2007); the G-dimer interface, which lies across the bound guanine nucleotide, and the NC-dimer interface, which is proximal to the N- and C-terminal helices (see Figure 1A). Thus, alternating G-dimer and NC-dimer interfaces provide a universal principle by which septins may assemble into heteromer units and extended filaments. The crystal structure of a complex derived from bacteria coexpressing SEPT2, SEPT6, and SEPT7, combined with electron microscopy, reveals a hexamer configured as a dimer of the trimeric SEPT2/6/7 unit (see Figure 1A; Sirajuddin *et al.*, 2007). Thus, while SEPT2 expressed alone forms homodimers that polymerize into filaments, the distribution of individual septins within the SEPT2/6/7 unit is nonrandom, that is, subunits are arranged as a perfect palindrome. The mechanism governing ordered heteromer assembly under conditions of coexpression is far from clear, but a recent study indicates the significance of alternating intrinsic GTPase activity among septin subunits (Sirajuddin *et al.*, 2009).

Mammalian septins are reportedly involved in diverse cellular functions, including chromosome segregation, cytokinesis, DNA damage response, cell migration, membrane dynamics, exocytosis, and apoptosis, as well as tumors and neurological disease states (reviewed in Peterson and Petty, 2010). Moreover, recent studies suggest a conserved function of septins as a diffusion barrier at the base of cellular appendages (Hu *et al.*, 2010; Kim *et al.*, 2010). Yet, it remains unclear whether these functions are linked to properties of specific family members or to the septin system as a whole. Several of the functional studies include data on the effect of depletion of individual septins via RNA interference. Some of these reveal that depletion of SEPT2 or SEPT7 may cause an associated degradation of other septins (Kinoshita *et al.*, 2002; Kremer *et al.*, 2005; Tooley *et al.*, 2009; Estey *et al.*, 2010). This hints that certain septins are nonexchangeable within stabilizing heterooligomers and/or higher-order filamentous structures. However, the interdependence between the multitude of vertebrate septins, as well as their native assembly states, remains poorly defined.

This study uses genetically manipulated human cells to define the rules that govern the native assembly states of septins. We found that septin family members are all assembled into a pool of stable heteromers exhibiting a minimum of six subunits. The data reveal patterns of interdependency that coincide with previously defined sequence homology subgroups of animal septins. We also provide evidence that an uneven distribution of the SEPT3-subgroup member SEPT9 among the core heteromers causes heterogeneity with respect to both subunit number and polymerization interfaces at ends.

RESULTS

Cell type–specific composition of septin family members

When coexpressed in *Escherichia coli*, the individual SEPT2, SEPT6, and SEPT7 proteins assemble into the head-to-head SEPT2/6/7 trimer arrangement depicted in Figure 1A, which may represent a protomer unit of higher-order filamentous septin structures (Sirajuddin *et al.*, 2007). Yet, the mammalian septin system is a composite of many differentially expressed gene products, which can be divided into four subgroups based on homology (Figure 1B). To establish septin expression profiles, we measured mRNA levels corresponding to all known septin proteins by quantitative real-time PCR (qRT-PCR) in three cell types (Figure 1B). The results reveal some differences, as well as similarities, between the HeLa (epithelial), K562 (undifferentiated myeloid), and Jurkat (T-lymphocytic) cell lines. The septins found to be significantly expressed in K562 cells were further examined by semiquantitative Western blotting, which revealed the expected correlation between mRNA and protein levels (Figure 1C). Due to lack of appropriate antibodies, the SEPT8 protein was not analyzed, but the mRNA level of this SEPT6 subgroup member predicts a comparably modest level in K562 cells.

Variable expression of SEPT5 and isoforms of SEPT9 are both notable differences between these cell types, with HeLa cells having undetectable levels of both SEPT5 and an ~40-kDa isoform of SEPT9 (termed $SEPT9^{40\ kDa}$; Figure 1C). Multiple isoforms of SEPT9 are caused by alternative splicing, and the small isoforms may lack large portions of either the N- or C-terminal ends (note that $SEPT9^{75\ kDa}$ is likely to include the SEPT9_v1 isoform; Peterson and Petty, 2010).

All septins behave similarly in their partitioning between soluble and insoluble states

It seems likely that higher-order septin assemblies are insoluble. To address the partitioning of individual septins between soluble and insoluble cellular fractions, K562 cells were gently permeabilized with saponin, followed by centrifugation to separate soluble proteins from the insoluble particulate cell fraction. Figure 2 shows the partitioning of selected proteins of K562 cells permeabilized either in a near-physiological ionic-strength buffer (Figure 2A) or in a buffer of lower ionic strength (Figure 2B).

Under either condition, we found the expected partitioning of a cytosolic marker protein, Op18, into the soluble fraction, and the intermediate filament protein vimentin into the particulate fraction (Figure 2, A and B). However, we observed that ionic strength has a profound effect on the partitioning of septins in permeabilized cells. Thus, all septins were released into a soluble fraction under conditions similar to those in Figure 2A, while ~50% of each of the septins was insoluble under low ionic-strength conditions similar to those in Figure 2B. The partitioning of septins is similar at 0°C and 20°C (Supplemental Figure S1). It is also noteworthy that the individual septin proteins behave similarly at the two conditions tested (Figure 2). Thus, based on the criteria of solubility in permeabilized cell populations at low ionic strength, all individual septins appear to contribute equally to insoluble structures.

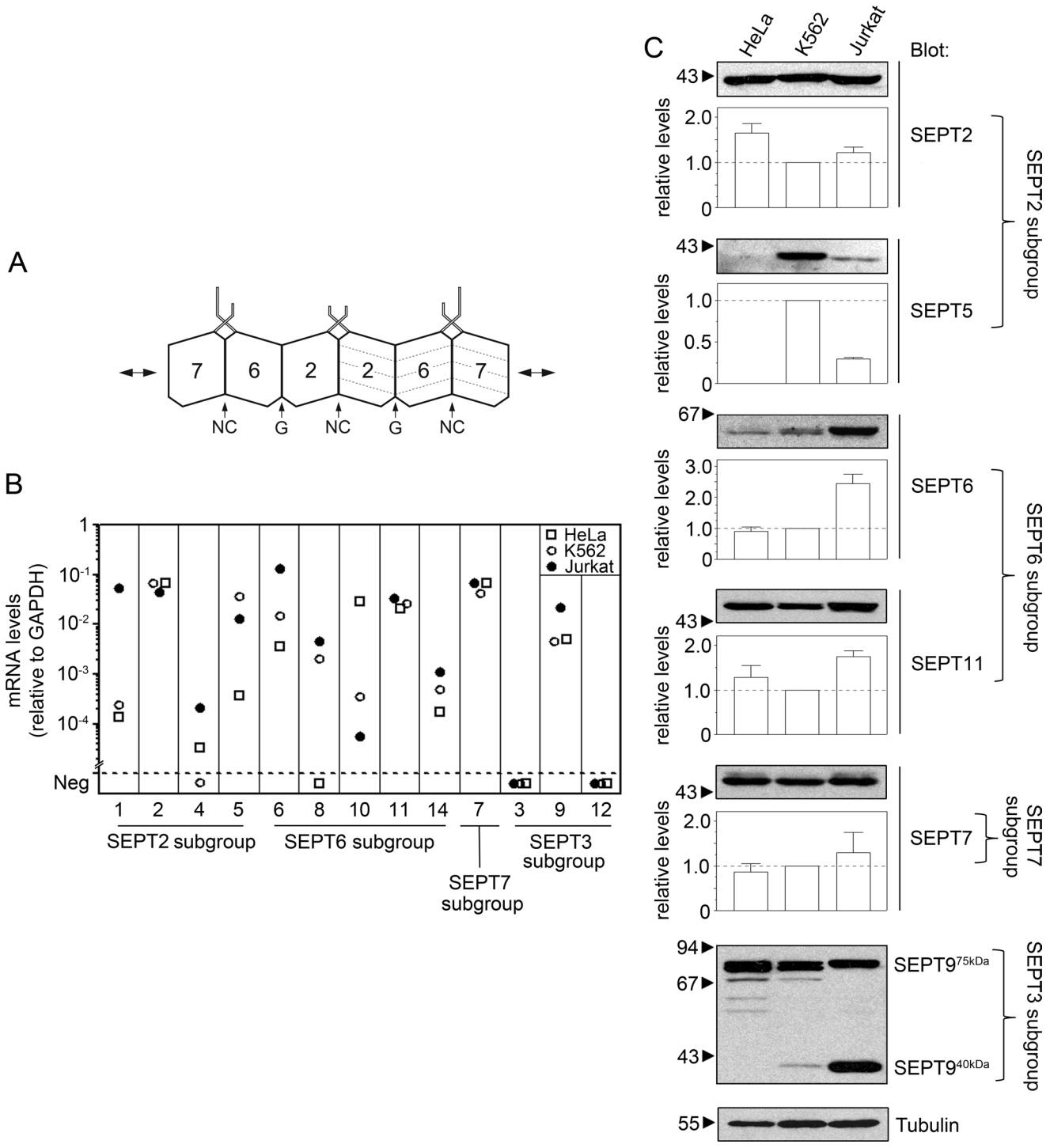

FIGURE 1: Septin expression profiles in epithelial (HeLa), myeloid (K562), and lymphoid (Jurkat) cell lines. (A) A schematic representation of a recombinant head-to-head SEPT2/6/7 trimer (PDB ID 2qag, dashed lines indicate different faces of trimer units). The hexameric SEPT7-SEPT6-SEPT2-SEPT2-SEPT6-SEPT7 unit has alternating G- and NC-dimer interfaces and filament assembly occurs through homodimeric SEPT7 G-dimer interfaces. The indicated C-terminal coiled-coil extensions serve to further stabilize the NC-dimer interface. (B) RNA was isolated from HeLa cells (open squares), K562 (open circles), and Jurkat (filled circles), and septin expression was screened using qRT-PCR. Septin mRNAs were internally normalized relative to glyceraldehyde 3-phosphate dehydrogenase. (C) A panel of anti-septin antibodies was used to screen crude extracts from the indicated cell lines. Isoforms of SEPT9 migrating close to the predicted SEPT9_v1 isoform at 75 kDa are all termed $SEPT9^{75\ kDa}$, and the isoform migrating at 40 kDa is termed $SEPT9^{40\ kDa}$. The SEPT9 antibody detects all isoforms, but the relative efficiencies may still vary. All data plotted are the means of triplicate determinations and are representative of at least three independent experiments.

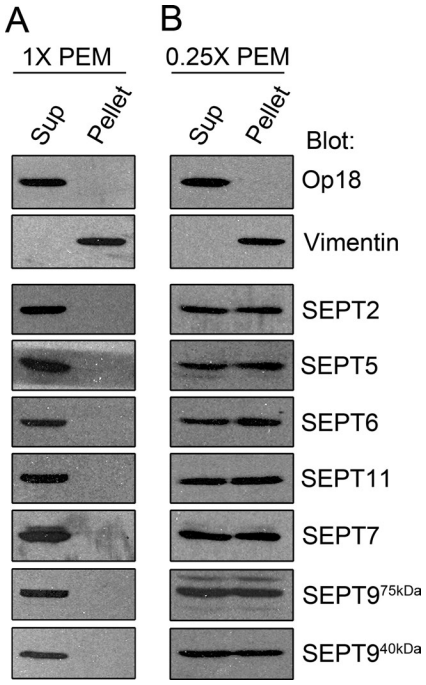

FIGURE 2: Partitioning of individual septin proteins between soluble and insoluble fractions of permeabilized cells. K562 cells were permeabilized by saponin in either 1X PEM at 0°C (A) or 0.25X PEM at 20°C (B) as outlined in *Materials and Methods*. The released (Sup) and cell-associated (Pellet) proteins were analyzed by Western blotting using the indicated antibodies. Data are representative of three independent experiments.

The disassembled septin system consists of a pool of relatively uniform complexes

The data on permeabilized K562 cells (Figure 2) were faithfully reproduced in similar experiments with HeLa and Jurkat cells (unpublished data). These findings indicate that all insoluble septin structures may rapidly disassemble into soluble components. To evaluate the size distribution of soluble septin-containing components, we used density-gradient centrifugation, followed by Western blot detection of individual septins. For accurate estimation of sedimentation coefficients, we calibrated gradients individually by mixing cell samples with standard proteins of known S value (Figure 3A).

Figure 3, B–D, shows sedimentation analysis of soluble septins prepared from HeLa, K562, and Jurkat cells under conditions that release all septins (i.e., as in Figure 2A). In all cases, the sedimentation profiles of soluble septin family members appeared symmetrical and well defined, and the peaks for individual septins coincided. While this analysis would not resolve minor size differences between specific septin complexes, a comparison with standard proteins indicates a relatively uniform pool of stable septin complexes with an average sedimentation coefficient around 8.1 S. Because the analysis is based on 16 h of centrifugation under dilute condition, essentially only stable complexes are resolved as symmetrical and well-defined peaks. It follows that the complexes characterized in Figure 3 have the anticipated stability of septin core heteromers. Note that all individual septins appear solely in the pool of stable heteromers.

SEPT6 subgroup members are interchangeable and represented in all heteromers

Most cell types express at least three of the five septins classified into the SEPT6 subgroup (see Figure 1B; Hall *et al.*, 2005). To

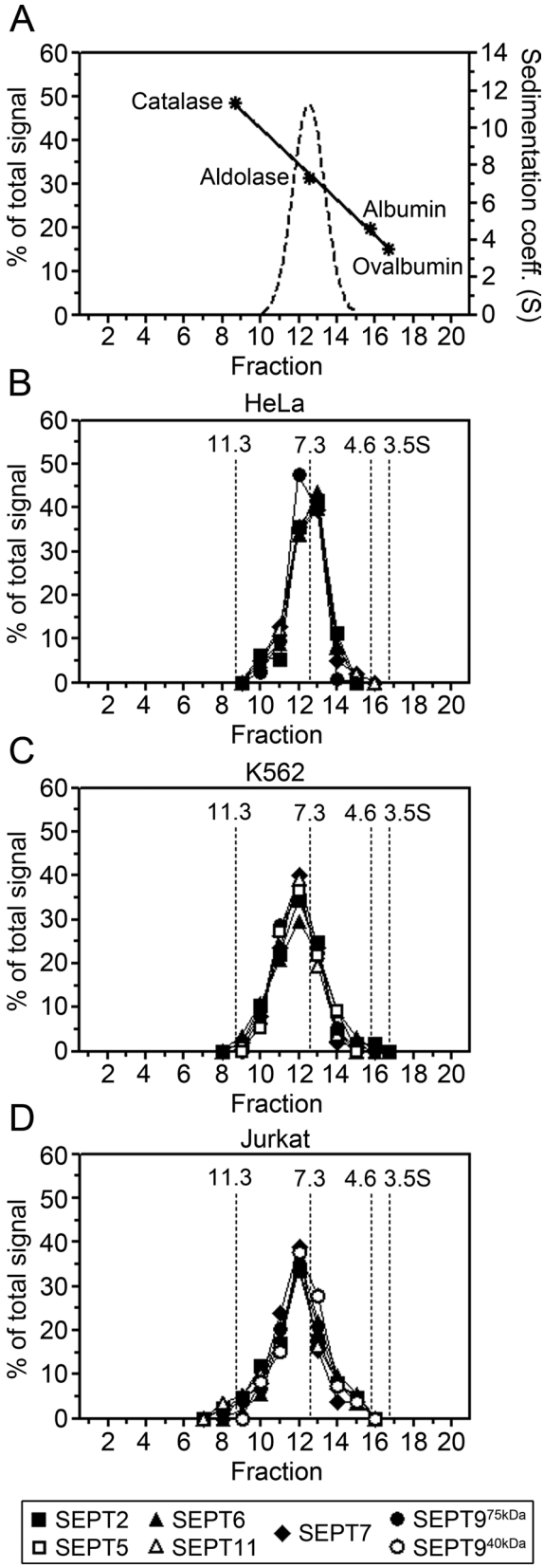

FIGURE 3: Density-gradient centrifugation analysis of septins in crude extracts. Septins released from permeabilized HeLa (B), K562 (C), and Jurkat (C) cells (protocol as in Figure 2A) were resolved by density-gradient centrifugation. The distribution of septins in fractions was analyzed by Western blot analysis using the indicated antibodies. The distribution of the 7.3 S aldolase standard is depicted in (A).

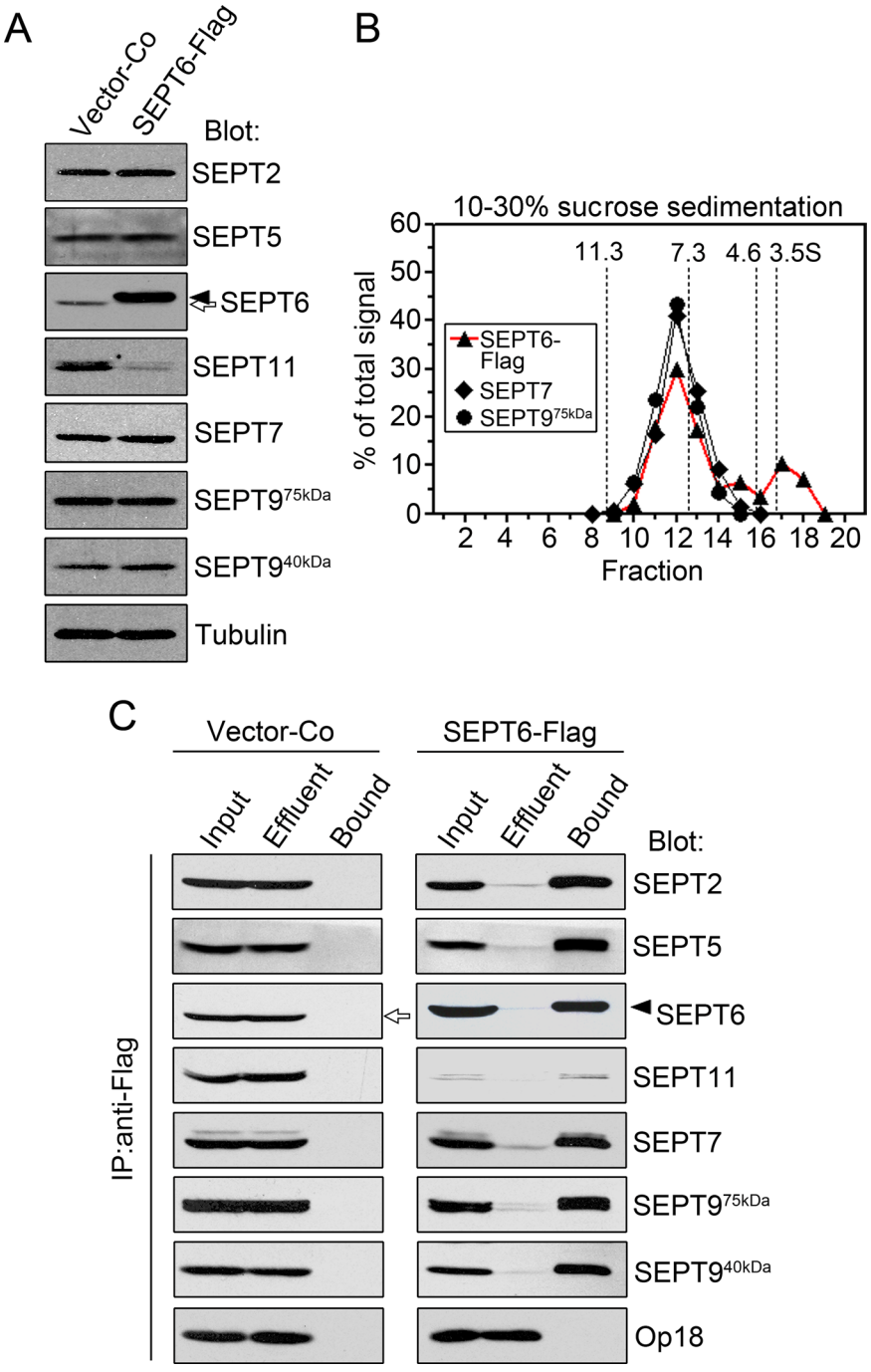

FIGURE 4: Analyses of endogenous septins in a cell line expressing the epitope-tagged SEPT6-Flag protein. K562 cells were transfected with a pMEP vector that directed inducible expression of SEPT6-Flag or an empty vector (Vector-Co) and counterselected with hygromycin, and expression was induced for 72 h. (A) Crude extracts were analyzed by Western blotting using the indicated antibodies (α-tubulin: loading control). (B) Septins released from permeabilized SEPT6-Flag–expressing cells (protocol as in Figure 2A) were resolved by density-gradient centrifugation, and the distribution of the indicated septins was analyzed as in Figure 3. The epitope-tagged SEPT6-Flag protein was detected by anti-Flag. (C) Septins released from permeabilized cells provided the starting material for affinity purification of SEPT6-Flag complexes by means of M2 anti-Flag–coupled beads (see *Materials and Methods*). Equivalent amounts of starting material (Input), unbound (Effluent), and FLAG-bead–captured (Bound) proteins of Vector-Co (left) or SEPT6-Flag–expressing cells (right) were analyzed by Western blotting using the indicated antibodies. Oncoprotein18 (Op18) was used as loading and specificity control. Data are representative of three independent transfection experiments.

address whether SEPT6 subgroup members are interchangeable within stable septin complexes, we analyzed K562 cells expressing an excess of a SEPT6 derivative with an eight-amino-acid FLAG epitope tag fused to the C-terminal coiled-coil extension (termed SEPT6-Flag). For regulatable expression and rapid selection of transfected cells, the episomally replicating pMEP4 vector was used. To ensure steady-state conditions of septin assembly, SEPT6-Flag was induced from the hMTIIa promoter over a 72-h period. As shown by Western blots in Figure 4A, expression of SEPT6-Flag appears specifically associated with selective degradation of SEPT6 subgroup proteins. Thus, while other septins are not affected, the levels of SEPT11 as well as the endogenous SEPT6 protein are severely decreased (note the slightly retarded migration of epitope-tagged SEPT6-Flag relative to endogenous SEPT6).

A simple interpretation of the results in Figure 4A is that SEPT6-Flag in excess competes specifically with endogenous SEPT6 subgroup members for coassembly into a limited number of core heteromers in which septins become stabilized; that is, SEPT6-Flag may selectively replace the SEPT6 subgroup members within heteromers. Consistent with this interpretation, sedimentation analysis reveals that the size distribution of the bulk of SEPT6-Flag–containing complexes coincides with the endogenous septins, as detected by SEPT7 and SEPT9 (Figure 4B), and is indistinguishable from those of endogenous septins in control K562 cells (Figure 3C). This analysis also revealed a ~20% subfraction of SEPT6-Flag with sedimentation properties consistent with a monomeric state (i.e., a peak close to 3.5 S as defined by the 43-kDa ovalbumin marker; Figure 4B). Given that SEPT6-Flag was expressed in sufficient excess to largely outcompete endogenous SEPT6 subgroup proteins from stabilizing complexes, the modest size of this subfraction suggests a rapid decay rate of monomeric SEPT6.

Septin complexes containing epitope-tagged SEPT6-Flag are retained by a FLAG antibody coupled to beads, which allows quantitative capture of such complexes from crude cell extracts. By this means, we could address the proportion of individual septins coassembled with SEPT6-Flag. Figure 4C shows Western blot analysis of equivalent amounts of starting material (Input), unbound (Effluent), and FLAG-bead–captured (Bound) proteins derived from either Vector-Co or SEPT6-Flag–expressing K562 cells. The specificity was confirmed by analysis of Vector-Co cells, which revealed undetectable amounts of bound septins. Importantly, in cells overexpressing SEPT6-Flag, we found that the FLAG beads efficiently depleted each one of the endogenous septins (including the residual amounts of the SEPT6 subgroup member SEPT11), which were

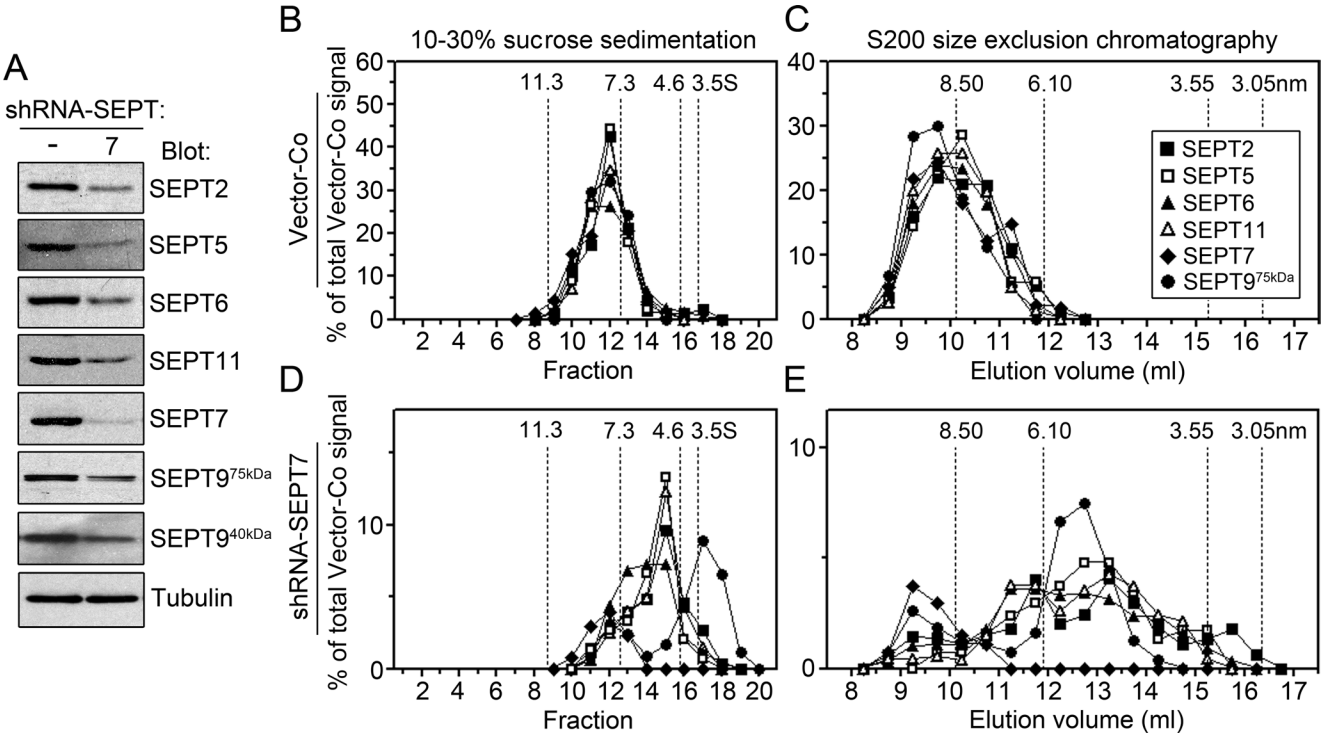

FIGURE 5: Quantitative and qualitative analyses of septin pools derived from Vector-Co or SEPT7-deficient cell lines. K562 cells were transfected with an RNA interference shuttle vector directing expression of shRNA-SEPT7, and counterselected with hygromycin for 1 wk. Septins released from permeabilized cells (protocol as in Figure 2A) were analyzed by Western blotting (A) or resolved by either density-gradient centrifugation (B and D) or gel-filtration chromatography (C and E). The distribution of septins in fractions was analyzed by Western blotting using the indicated antibodies. The peaks of standard proteins used for determination of sedimentation coefficients and Stokes radius are indicated in (B–E).

all recovered in the bound fraction (>90% recovery). Thus, the entire pool of septin complexes contains at least one SEPT6-Flag subunit.

Based on the present analysis, it can be concluded that SEPT6 subgroup members are interchangeable during assembly of heteromer units, which reveals the significance of this subgroup classification. Our data are also consistent with the notion that native septins exist solely in the context of SEPT6 subgroup–containing heteromers.

Septins exist solely in the context of heteromers that depend on SEPT7 for stability

Our strategy for continual depletion of specific septins is based on RNA interference by short hairpin RNA (shRNA), expressed by an episomally replicating viral vector, which confers hygromycin resistance. Semistable shRNA-expressing cell lines could be selected within a few days, which facilitated scoring of end-term phenotypes in terms of hydrodynamic parameters of the remaining septins. Figure 5A shows that expression of an shRNA derivative targeting SEPT7 mRNA (termed shRNA-SEPT7) in K562 cells results in efficient depletion of the SEPT7 protein, which is the sole member of its subgroup in all cell types (see Figure 1B). In accordance with previous reports (Kinoshita *et al.*, 2002; Kremer *et al.*, 2005; Tooley *et al.*, 2009; Estey *et al.*, 2010), an associated decrease of all other septin proteins was also observed. However, in contrast to reported effects on adhesion substrate–dependent cell lines (reviewed in Weirich *et al.*, 2008), we did not detect that SEPT7 depletion in nonadherent cell lines (e.g., K562 of Jurkat), interfered with cell division, or decreased the proliferation rate (unpublished data).

Consistent with data in Figure 3C, sedimentation analysis in Figure 5B shows that septins derived from the K562 Vector-Co cell line were all included in complexes with similar sedimentation profiles corresponding to an average sedimentation coefficient of ~8.1 S. Moreover, gel-filtration chromatography (Figure 5C) revealed indistinguishable elution profiles for all septins, except SEPT9, with average peak positions corresponding to a Stokes radius of ~9 nm. The hydrodynamic parameters, that is, ~9 nm and ~8.1 S, correspond to elongated complexes with an average mass of ~306 kDa, which is close to the deduced 282-kDa mass of a hexameric SEPT2/6/7 unit. Even so, the gel-filtration profiles also suggest SEPT9-containing subpopulations (>9 nm) of septin complexes.

Analysis of shRNA-SEPT7–expressing cell lines in Figure 5A revealed ~90–95% decrease in SEPT7 levels, while other septins were reduced by 65–75%. This decrease of individual septins is also mirrored in sedimentation and gel-filtration profiles presented in Figure 5B–E (compare *y*-axis scales). Given persistent SEPT7 depletion, these profiles reflect the hydrodynamic parameters of residual septins under steady-state conditions. It is notable from sedimentation (Figure 5D) and gel-filtration (Figure 5E) profiles that the residual SEPT7 is only detectable in the severely diminished pool of normal-sized complexes, while the bulk of SEPT2 and SEPT6 subgroup septins are all contained within aberrantly small complexes. In addition, the sedimentation profiles show that SEPT9 does not coexist with other septins in the absence of SEPT7 (Figure 5D). Consistent with these data, gel-filtration elution profiles reveal a well-defined peak of SEPT9, while SEPT2 and SEPT6 subgroup septins elute as coinciding broad peaks corresponding

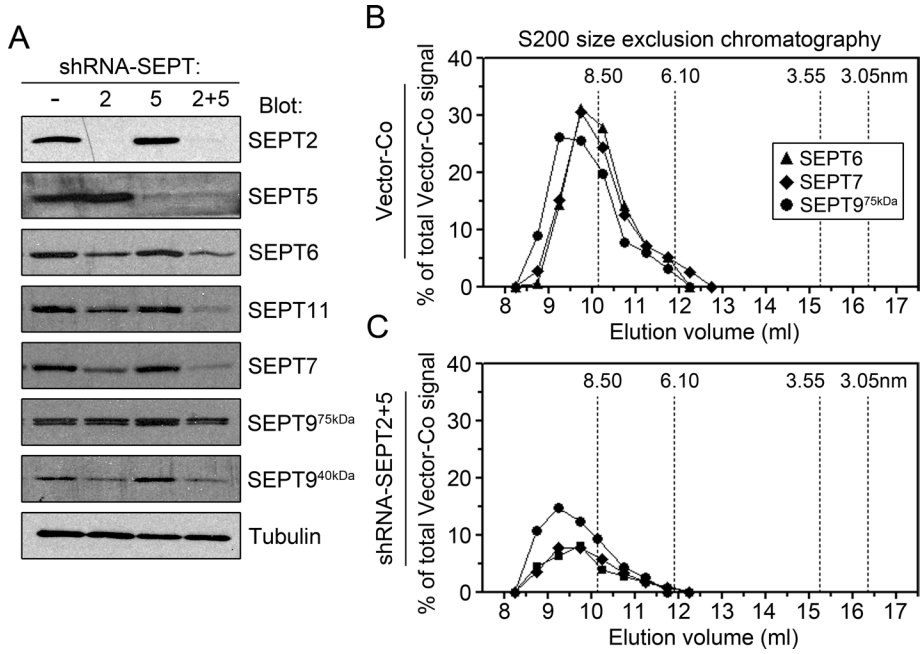

FIGURE 6: Quantitative and qualitative analyses of septin pools derived from SEPT2 subgroup–deficient cell lines. K562 cells were cotransfected with shRNA-SEPT2 and shRNA-SEPT5 as in Figure 5. Septins released from permeabilized cells were analyzed by Western blotting (A) or resolved by gel-filtration chromatography (B and C), as in Figure 5. The elution profiles of SEPT6, SEPT7, and SEPT9$^{75\ kDa}$ derived from Vector-Co (B) and SEPT2 subgroup–deficient cells (C) are shown.

to aberrantly small and heterogeneous complexes (Figure 5E). In the absence of SEPT7, the hydrodynamic parameters of SEPT9$^{75\ kDa}$ (~3.2 S and ~5.8 nm) correspond to ~78 kDa and an elongated shape, which suggests a monomeric state.

We found that the level of residual, normal-sized septin complexes in SEPT7-deficient cells can be accounted for by the 5–10% basal level of the remaining SEPT7. These results indicate that all septins exist solely as subunits of SEPT7-containing heteromers in their native state. Moreover, under experimental conditions of diminishing SEPT7 content, the assembly states of SEPT2 and SEPT6 subgroup members is clearly different from SEPT9. It is evident from the present data that SEPT9 depends on SEPT7 for assembly into any form of stable heteromers. The specificity of this phenotype was confirmed by successful complementation of shRNA-SEPT7–expressing cells with an epitope-tagged SEPT7 derivative with silent point mutations within the shRNA-targeting sequence (unpublished data).

The result of a corresponding analysis of Jurkat cells was also consistent with SEPT7 depletion leading to monomers of SEPT9 and aberrantly small heteromers of SEPT2 and SEPT6 subgroup septins (Figure S2). It is evident from data in Figure 5 that the hydrodynamic parameters of these aberrant heteromers are poorly resolved, in particular by gel filtration. Given that well-resolved hydrodynamic parameters require stable complexes, the poor resolution may at least in part be due to decay of aberrant heteromers that are less stable than native heteromers. Nevertheless, the sedimentation profiles still suggest that a significant proportion of the SEPT2 and SEPT6 subgroup septins are arranged as tetrameric heteromers in SEPT7-deficient cells.

The SEPT2 subgroup appears essential for initiating assembly of septins into stabilizing heteromers

K562 cells express high levels of two SEPT2 subgroup members, namely SEPT2 and SEPT5 (see Figure 1B). To address a potential subgroup-specific functional significance, K562 cell lines expressing shRNA-SEPT2 and/or shRNA-SEPT5 were established by the same general strategy as in Figure 5. Western blots in Figure 6A reveal efficient depletion of either SEPT2 (~90%) or SEPT5 (~75%), and depletion of both septins by coexpression of the two shRNA derivatives. Moreover, it is also shown that depletion of either SEPT2 or SEPT5 results in only a modest decrease in the content of other septins, while codepletion results in ~75% reduction of all other septins, except SEPT9$^{75\ kDa}$, the major SEPT9 isoform in K562 cells, which was markedly less affected.

Gel-filtration elution profiles of septin complexes in Vector-Co and SEPT2 subgroup–depleted cells are shown in Figure 6, B–C. Detection of the remaining SEPT6, SEPT7, or SEPT9$^{75\ kDa}$ in cells depleted of either SEPT2 or SEPT5 alone (Figure S3), or in combination (Figure 6C), reveals only heteromers within the normal size range. Thus, diminishing heteromer content is not associated with aberrantly small complexes or monomers of residual septins. These data suggest a generic SEPT2 subgroup–specific function during an early step of the heteromer assembly process.

The combined data in Figures 5 and 6 may be interpreted as evidence for a SEPT2 subgroup–specific role to stabilize SEPT6 subgroup members in tetrameric assembly intermediates, which are subsequently capped by SEPT7 at the ends. However, an assembly model exclusive to such hexameric heteromers does not explain the data related to SEPT9. Thus, residual SEPT9 exists as monomers in SEPT7-deficient cells (see Figure 5, D and E), but not in SEPT2 subgroup–deficient cells (Figure 6C), and heteromers containing SEPT9 appear to comprise a subpopulation that is somewhat larger than the average of heteromers defined by detection of all the other septins (see Figures 5C and 6B).

A comparison of gel-filtration profiles in Figures 5 and 6 requires that the differences in the relative decrease of normal-sized heteromers are considered. Thus, as judged by detection of SEPT6 and/or SEPT7, shRNA-SEPT7–expressing cells contain only ~5–10% of residual normal-sized heteromers (note difference in scales in Figure 5, C and E), while shRNA-SEPT2/shRNA-SEPT5–expressing cells contain 25–35% residual heteromers. Thus, given the evidence for substoichiometric amounts of SEPT9, a substantial fraction of the available SEPT9 can be expected to become assembled into core heteromers in shRNA-SEPT2/shRNA-SEPT5–expressing cells, but not in shRNA-SEPT7–expressing cells. The slight shift in gel-filtration profiles of shRNA-SEPT2/shRNA-SEPT5–expressing cells toward a larger Stokes radius and a substantial increase in the relative SEPT9 content of residual heteromers indicate that this is indeed the case (compare Figure 6, B and C). In accordance with this interpretation, the data in Figure 6C indicate that the gel-filtration profile of SEPT9 coincides with the profiles based on detection of either SEPT6 or SEPT7. These results are consistent with the fact that SEPT9 under normal circumstances is present in substoichiometric amounts and, most importantly, that SEPT9 is a distinguishing subunit that makes a subpopulation of heteromers larger.

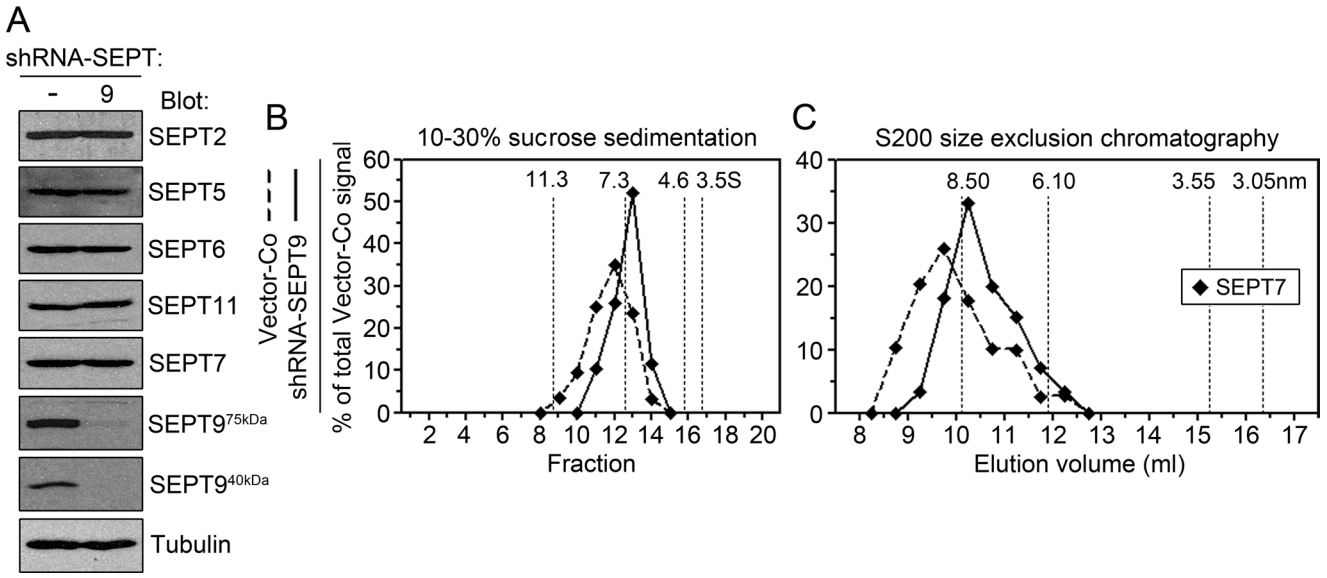

FIGURE 7: Quantitative and qualitative analyses of the septin pool derived from SEPT9-deficient cell lines. K562 cells were transfected with shRNA-SEPT9, as in Figure 5. Septins released from permeabilized cells were analyzed by Western blotting (A) or resolved by either density-gradient centrifugation (B) or gel-filtration chromatography (C), as in Figure 5. The elution profiles of SEPT7 derived from Vector-Co (dashed lines) and shRNA-SEPT9 (solid lines) are shown in (B and C).

SEPT9 depletion results in a more uniform heteromer pool with a decreased average mass

To directly address the significance of SEPT9 for the size distribution of septin heteromers, we established K562 cell lines expressing shRNA-SEPT9 in which both the SEPT9$^{75\ kDa}$ and SEPT9$^{40\ kDa}$ isoforms were depleted by >90% (Figure 7A). While all other septins appeared unaffected in terms of protein content (Figure 7A), sedimentation analysis suggests a more uniform heteromer pool in SEPT9-deficient cells with a peak corresponding to a slightly decreased sedimentation coefficient (Figure 7B). Comparison of gel-filtration elution profiles indicates a specific decrease of heteromers with a Stokes radius >9 nm. The data in Figure 7 are based on detection of SEPT7; however, the results were reproduced in a detection of SEPT2 or SEPT6 subgroup members (unpublished data).

The hydrodynamic parameters of heteromers in SEPT9-deficient cells (~7.3 S and ~8.4 nm) correspond to an average mass of ~254 kDa, which should be compared with ~306 kDa in control cells (~8.1 S and ~9.0 nm) and the deduced 282-kDa mass of a hexameric SEPT2/6/7 unit. Given that SEPT9 depletion also results in somewhat more uniformly sized heteromers, these data suggest that SEPT9-containing heteromers represent a subpopulation with more than six subunits in which all four septin subgroups are represented.

A strategy for rapid isolation of the endogenous pool of septin heteromers

Our strategy for purification of endogenous septin heteromers relied on two premises: 1) the endogenous SEPT7 protein is rapidly degraded if it is not coassembled with the appropriate septin subgroup members (see Figure 6), and 2) SEPT7 is a subunit in all septin heteromer units (see Figure 5). The purification strategy involved replacement of endogenous SEPT7 during heteromer assembly by means of stable expression of a SEPT7 derivative designed to allow efficient affinity purification. For this purpose, we used an analogous approach, as described for expression of epitope-tagged SEPT6 (see Figure 4). The Western blots in Figure 8A are consistent with SEPT7-Flag expression results in a specific gene-product replacement. Thus, several days of SEPT7-Flag expression causes degradation of the endogenous SEPT7 protein without detectably altering protein levels of other septins (note retarded migration of epitope-tagged SEPT7-Flag relative to endogenous SEPT7). Moreover, sedimentation analysis shows that SEPT7-Flag has to a large extent replaced the endogenous gene product in heteromers, and we did not detect any SEPT7-containing species of aberrant size (Figure 8B).

SEPT7-Flag–containing heteromers were isolated by means of a FLAG-specific antibody coupled to beads and then underwent competitive elution with a FLAG peptide. The major fraction of all septins (~80%) was retained on beads and specifically eluted by the peptide (unpublished data). As shown in Figure 8C, a Coomassie Blue–stained SDS–PAGE gel identified proteins corresponding to the septins listed in the margin, as confirmed by Western blotting. Figure 8C also shows that SEPT9$^{75\ kDa}$ is undetectable in heteromers isolated from a SEPT9-deficient K562 cell line in which shRNA-SEPT9 was coexpressed with SEPT7-Flag. Finally, the abundance of SEPT9 in nondepleted cells (i.e., the sum of the SEPT9$^{75\ kDa}$ and the barely detectable SEPT9$^{40\ kDa}$ isoforms) appears significantly lower than each of the three other subgroups, which is consistent with our evidence that SEPT9 defines heteromer subpopulations.

Based on the present analysis of affinity-purified septin heteromers, it can be estimated that the entire septin pool comprises ~0.1% of all cytosolic proteins. This estimate is consistent with independent estimates based on quantitative Western blotting using recombinant septins as standard (unpublished data). Thus, septins are far less abundant than a cytoskeletal protein such as tubulin, which constitutes ~2% of cytoplasmic proteins in K562 cells (Sellin *et al.*, 2008).

SEPT9 is present only in stable heteromers with more than six subunits

The size distribution of the immunoaffinity-purified septin heteromers characterized in Figure 8 was determined using electron microscopy. Electron micrographs of negatively stained preparations derived from SEPT7-Flag–expressing control (Figure 9A) and

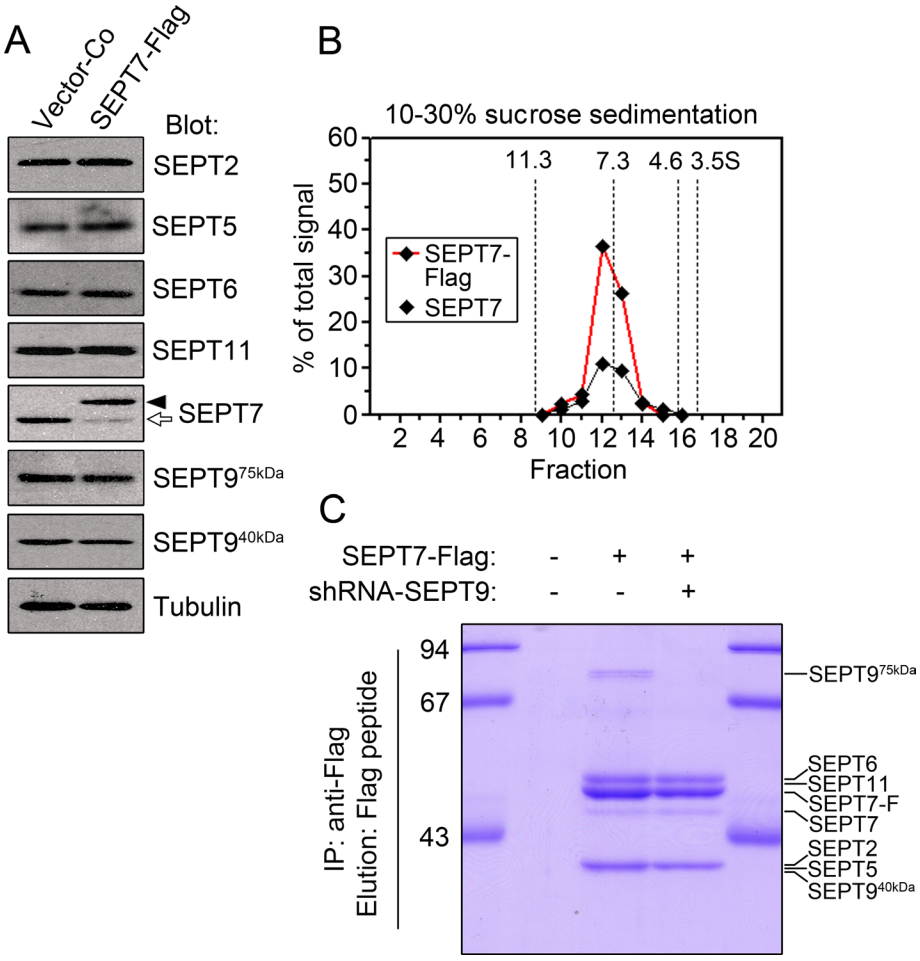

FIGURE 8: Replacement of endogenous SEPT7 with epitope-tagged SEPT7-Flag and analysis of affinity-purified endogenous septin heteromers. A transfected K562 cell line was induced to express the SEPT7-Flag protein over a 1-wk period. Septins released from permeabilized cells were analyzed by Western blotting (A) or resolved by density-gradient centrifugation (B). Septins released from permeabilized cells provided the starting material for affinity purification of SEPT7-Flag complexes by means of M2 anti-Flag–coupled beads (C). The Coomassie Blue–stained SDS–PAGE gel shows specifically bound proteins from Vector-Co (lane 1), SEPT7-Flag (lane 2), or SEPT7-Flag/SEPT9-deficient cells (lane 3). Proteins corresponding to 40×10^6 cells were loaded in each lane. Note that the DYKDDDDK sequence of the FLAG-tag binds tightly to Coomassie Blue, which skews the impression of the SEPT7-Flag ratio relative to endogenous septins.

SEPT9-depleted cells (Figure 9C) reveal in both cases the expected rod-shaped particles. Determination of the length distribution of particles from control cells reveals heterogeneity, but the peak of the major category is in the range of 26–28 nm (Figure 9B). This agrees well with the reported ~27-nm length of the major category of rat brain–derived septin heteromers, which was shown by image processing to represent hexamers (Lukoyanova *et al.*, 2008). Thus, a large fraction of all heteromers have a length distribution consistent with hexamers, in which each subunit corresponds to ~4.5 nm, as indicated by arrowheads in Figure 9B.

The population of the longest rods in control cells is relatively heterogeneous, but the distribution peaks between 34 and 35 nm (Figure 9, A and B). Given the estimated ~4.5 nm per septin subunit of hexamers, this peak agrees well with the predicted 36-nm length of octamers. In addition, the length distributions of rods also give an impression of a minor population with a length distribution consistent with heptamers, but this putative heteromer population is poorly resolved (Figure 9B).

Figure 9, C and D, demonstrates that SEPT9 depletion alters the length distribution of rods. Thus, the particles in these preparations have a length distribution with a single peak between 27 and 28 nm, which corresponds to hexamers, and the fraction of rods with a length corresponding to larger heteromers is essentially abolished. Thus, consistent with hydrodynamic data presented above (Figures 5, 6, and 7), SEPT9-containing heteromers represent subpopulations of core heteromers with more than six subunits. The combined data in this study are summarized in a generic model for heteromer assembly (Figure 10).

DISCUSSION

This study has examined the composition of the protomer units that serve as a pool of building blocks for higher-order septin structures. Our results support three main conclusions: 1) human septins exist solely in the context of six- to eight-subunit core heteromers, all of which contain SEPT2 and SEPT6-subgroup members and SEPT7, while heteromers comprising more than six subunits also contain the SEPT3 subgroup member SEPT9; 2) heteromer arrangements appear linked to subgroup-specific properties that govern the temporal order of heteromer assembly; and 3) polymerization into filaments may involve both NC- and G-dimer interface interactions at core heteromer ends. These conclusions are integrated into the model in Figure 10. In the following sections, we discuss the evidence that supports each of these conclusions.

The composition and assembly state of septin family members in different cell types

Delineation of native assembly states and interdependencies of mammalian septins is complicated by the sheer number of genes, most of which are differentially expressed in various cell types. In this study, we quantified mRNA levels of all 13 functional septin genes in human cell lines representing epithelial, hematopoietic, and lymphoid cell types (Figure 1B). Despite some notable differences in septin composition, the three cell types are similar with respect to the partitioning of individual septins between soluble and insoluble states (unpublished data) and the size range of soluble septin protomer units (Figure 3). In addition, the total content of septin proteins also appeared to be essentially the same (Figure 1C; note similar SEPT7 content), which was estimated to ~0.1% of total cellular proteins in K562 cells (Figure 8). Thus, while the analysis of genetically manipulated cells was limited to K562 and Jurkat, it seems likely that our general conclusions also apply to other human cell types.

To set the premises for characterization of the complete protomer unit pool, we evaluated septin partitioning between soluble and insoluble states in asynchronously growing cells. These analyses did not reveal any differences in the proportional

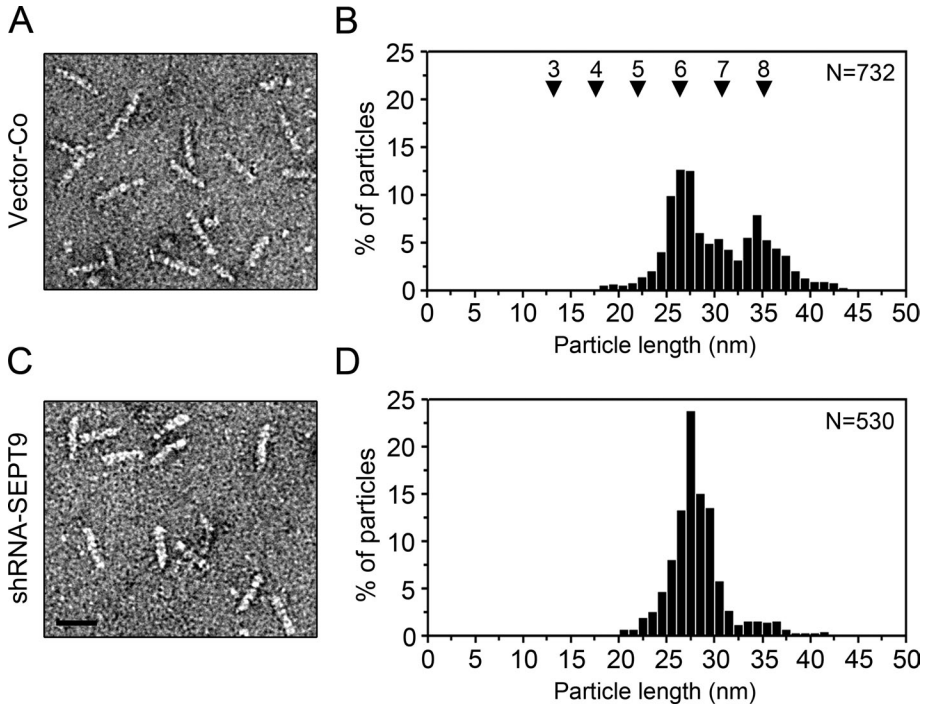

FIGURE 9: Negative-stain electron microscopy of endogenous septin heteromers prepared from control and SEPT9-deficient cell lines. Heteromers from K562 cells expressing SEPT7-Flag alone (A and B) or in combination with shRNA-SEPT9 (C and D) were affinity-purified by the strategy described in Figure 8. Images of representative fields of the grid are shown in (A and C) and histograms of the length distribution of rod-shaped particles are shown in (B and D). The histograms represent the length interval 16–44 nm. Scale bar: 25 nm.

distribution of individual septins between these two states (Figure 2). The insoluble state appears to represent labile higher-order structures, since cell permeabilization in a near-physiological ionic-strength buffer was sufficient for quantitative recovery of all septins in a soluble fraction. Even so, the hydrodynamic properties of septin species at this ionic strength reveal an asymmetrical distribution, indicating incomplete disassembly into protomer units (unpublished data). However, by addition of 0.3 M NaCl to buffers used for sedimentation and gel filtration, the size distribution of all septins became relatively uniform and symmetrical, thus indicating complete disassembly into a pool of stable oligomer units (Figures 3 and 5). Considering the time span required for completion of the gradient centrifugations and gel-filtration analysis, as well as dilution in high-ionic-strength buffers, it can be assumed that essentially only stable complexes are resolved as symmetric peaks. Nevertheless, there was still no evidence for decay products among septin heteromers. In addition, we did not detect any time-dependent alterations in the ratio between six- and eight-subunit heteromers in crude cytosolic preparations (unpublished data). This supports one general conclusion of this study, namely that septin proteins exist only in the context of a repertoire of stable core heteromers in HeLa, K562, or Jurkat cells.

Septin subgroup–specific interdependencies during assembly into stable heteromers

Structural studies of mammalian septins have largely focused on complexes formed upon recombinant expression of various combinations of SEPT2, SEPT6, and SEPT7 proteins (Kinoshita *et al.*, 2002; Sheffield *et al.*, 2003; Low and Macara, 2006; Sirajuddin *et al.*, 2007, 2009). In contrast to SEPT6 and SEPT7, recombinant SEPT2 forms dimers that in turn polymerize into homotypic filaments (Mendoza *et al.*, 2002; Huang *et al.*, 2006; Sirajuddin *et al.*, 2007). It is notable that recombinant SEPT2 in solution exists as stable G-interface homodimers; while SEPT2 is dimerized through the NC-interface when coexpressed with SEPT6 and SEPT7 (see Figure 1A; Sirajuddin *et al.*, 2007). In addition, recombinant coexpression of SEPT6 and SEPT7, as well as SEPT2 and SEPT7, results in stoichiometric binary complexes (Sheffield *et al.*, 2003). Thus, while coexpression of the SEPT2, SEPT6, and SEPT7 proteins results in ordered assembly into a head-to-head SEPT2/6/7 trimer arrangement; pairing of recombinant septins may still be fairly promiscuous.

In this study, we have addressed the rules governing the native assembly state of septins by strategies involving either regulatable overexpression or persistent depletion (by RNA interference) of selected septins. The data reveal patterns of interdependencies between individual septins that in light of structural studies of recombinant septin complexes suggest a model for ordered assembly into heteromers. According to the model (Figure 10), the temporal order of assembly according to homology subgroups directs the arrangement of the final heteromer.

Expression of epitope-tagged SEPT6-Flag demonstrates subgroup-restricted degradation of endogenous SEPT6 and SEPT11 by a mechanism involving competition for heterooligomerization partners (Figure 4). During revision of this report, we have also confirmed that SEPT8 is degraded (unpublished data). The same principle mechanism also allows efficient replacement of endogenous SEPT7 with SEPT7-Flag within the heteromer pool without accumulation of monomeric SEPT7 (Figure 8). Our results suggest that both SEPT6-Flag and SEPT7-Flag coassemble in a subgroup-specific manner into the entire pool of heteromers without altering the size distribution, which supports a key aspect of our model, namely that SEPT2 and SEPT6-subgroup members and SEPT7 are represented in all native heteromers. Finally, the present data also support that assembly into heteromers is essential for the structural integrity of both SEPT6 subgroup members and SEPT7.

The first part of our model is based on the evidence that the two SEPT2 subgroup members in K562 cells, SEPT2 and SEPT5, share an essential function required to initiate septin assembly under native conditions. It is assumed in the model (Figure 10, step 2) that SEPT2 subgroup members nucleate heteromers through G-interface interactions with monomeric SEPT6 subgroup members. The evidence that SEPT2 and SEPT6 subgroup members form tetrameric assembly intermediates include: 1) that SEPT7-deficient cells contain appreciable amounts of partial heteromers of SEPT2 and SEPT6 subgroup members within a size range consistent with tetramers, while residual SEPT9 exists as monomers (Figure 5); 2) consistent with a shared function within the SEPT2 subgroup, single depletion of either SEPT2 or SEPT5 results only in modest reductions of septins belonging to other subgroups (Figures 6A and S3); and 3) codepletion of SEPT2 and SEPT5 causes a severe decrease of heteromer content, but under these

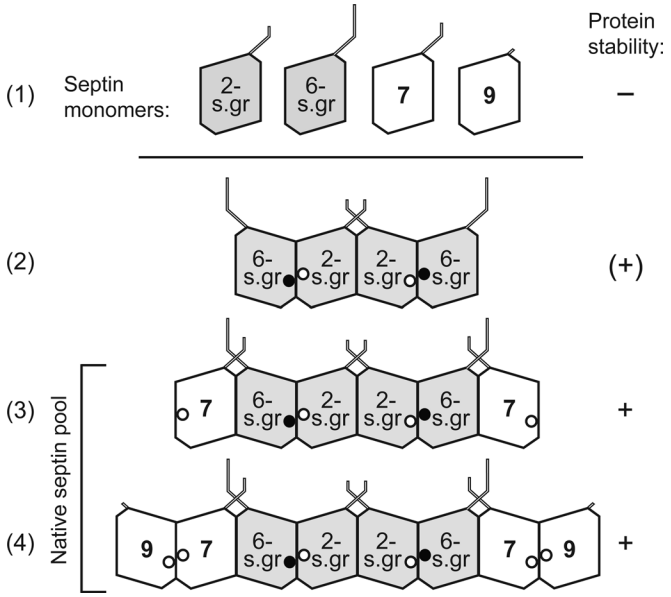

FIGURE 10: A model of how the temporal order of septin assembly directs the subunit arrangement according to homology-based subgroups. Shaded subunits represent any member of either the SEPT2 (2-s.gr) or SEPT6 (6-s.gr) subgroups, while open subunits represent the individual SEPT7 or SEPT9 gene products, since only a single subgroup member exists within the cell model systems. Step 1 depicts newly synthesized unstable monomers. Step 2 depicts a partially stable tetrameric assembly intermediate, which requires capping by SEPT7 at both ends to become completely stable, as shown in step 3. In step 4, subpopulations of octamers (possibly also heptamers) arise by coassembly of substoichiometric amounts of SEPT9 isoforms at ends of hexamers. The subgroup arrangement of tetramers (step 2) is based on the solved structure of the recombinant SEPT2/6/7 trimer (GTP = closed circles; GDP = open circles). Hexameric units have G-interfaces at their ends (i.e., according to the solved structure of the hexamer configured as a dimer of the trimeric SEPT2/6/7 unit), while octameric units are depicted with NC-interfaces at their ends, which would predict a mixture of polymerization interfaces among core heteromers. However, it remains possible that octameric units are arranged as, e.g., hexamers with a SEPT9 dimer at one end, which would imply G-interfaces at both ends.

conditions there were no indications of partial heteromers of residual septins (Figure 6).

The tetramers of SEPT2 and SEPT6 subgroup members observed in SEPT7-deficient cells are clearly less stable than native hexamers. Capping by SEPT7 at both ends is therefore a likely next step in the assembly process, which results in a pool of stable hexamers (Figure 10, step 3). A fraction of these hexamers coassembles with substoichiometric amounts of the SEPT3-subgroup member SEPT9 to generate subpopulations of octamers (Figure 10, step 4), and possibly also heptamers (Figure 9B). It is assumed in our model that no reshuffling of the subunit order has occurred in SEPT9-containing heteromers; that is, SEPT9 is placed adjacent to SEPT7 at the heteromer ends. The evidence supporting this model for the genesis of SEPT9-containing subpopulations of heteromers includes: 1) residual SEPT9 exists as a monomer in SEPT7-deficient cells (Figure 5, D and E), which indicates a SEPT7–SEPT9 interface; 2) a partial depletion (~75%) of the SEPT2 subgroup, which results in the corresponding quantitative decrease of the total heteromer content, saturates the residual heteromers with SEPT9-subunits (Figure 6); and 3) SEPT9-depletion abolishes the subpopulations of large heteromers, as evidenced by gel filtration (Figure 7) and single particle analysis (Figure 9), but the total heteromer content and the relative content of all other septins appear unaltered (Figures 7 and 8).

The ubiquitously expressed *SEPT9* gene produces a multitude of splicing variants, and there is evidence for up to 15 distinct SEPT9 polypeptides (Peterson and Petty, 2010). These splice forms differ in their N- or C-termini, but not in the conserved G-domain. HeLa and K562 cells predominantly express the largest SEPT9 isoforms, that is, SEPT9$^{75\ kDa}$, but a small SEPT9$^{40\ kDa}$ isoform is abundant in Jurkat cells (Figure 1B). Notably, sedimentation analysis or gel filtration does not distinguish heteromer containing SEPT9$^{75\ kDa}$ and SEPT9$^{40\ kDa}$, and these isoforms appeared equally reduced and were both present as monomers in SEPT7-deficient cells (Figures 3, 5, and S2). However, under conditions of an experimentally decreased heteromer pool (i.e., partial SEPT2 subgroup depletion), the content of the SEPT9$^{40\ kDa}$ isoform is comparably more reduced than SEPT9$^{75\ kDa}$ (Figure 6A). Thus SEPT9$^{75\ kDa}$ appears favored over the SEPT9$^{40\ kDa}$ isoform during coassembly with substoichiometric amounts of stabilizing heteromers, which is the only difference we have so far detected between these isoforms.

The hexameric unit of the recombinant SEPT2/6/7 complex appears as an ~25 nm rod under an electron microscope (Sirajuddin *et al.*, 2007). Similar analysis of native septin heteromers purified from *Drosophila* indicates a length distribution of heteromer units with a single peak at ~26 nm. Based on hydrodynamic data, it was proposed in this early study that the identified heteromer unit of septin filaments is a hexamer (Field *et al.*, 1996). Notably, *Drosophila* lacks representatives of the SEPT3-subgroup and an apparently uniform heteromer pool of hexamers is therefore consistent with the model in Figure 10. Moreover, a detailed classification of images of rat brain heteromers has indicated a major 27-nm group and a second 32-nm group, but unambiguous separation of these two groups was precluded due to a low signal-to-noise ratio (Lukoyanova *et al.*, 2008). These estimates agree well with the average length of the predicted hexamers and octamers in this study (Figure 9). However, the claim that heteromers isolated from rat brain consist solely of three individual septins, SEPT3, SEPT5, and SEPT7, seems contradictory to our data and to previous studies in which immunoprecipitation of individual septins from mouse brain or mammalian cell lines was shown to result in coprecipitation of every other septin (Kinoshita *et al.*, 2002; Tooley *et al.*, 2009). It appears to us that the stated septin composition of rat brain–derived heteromers is flawed by misannotation, e.g., the band annotated as SEPT5 migrates as a SEPT6 subgroup member on SDS–PAGE gel.

It is noteworthy that previous immunoaffinity purification of SEPT2 containing heteromers from mouse brain resulted in heteromers containing at least 10 individual septin polypeptides, which included all four SEPT2 subgroup members (Kinoshita *et al.*, 2002). While these preparations were analyzed by electron microscopy and gel filtration in low-salt (75 mM KCl), they were generated under conditions involving extensive high-salt washing steps (up to 1 M KCl), which, according to our data, is more than enough for complete disassembly into core heteromer units. Thus these previous data suggest heterodimerization of SEPT2 subgroup members, which is in line with our conclusion that the native pool of six- to eight-subunit core heteromers is a composite of an array of heteromers that are assembled according to homology subgroups, and consequently not arranged as perfect palindromes.

Concluding remarks

Individual septins have commonly been implicated in some particular function of mammalian cells, or as interaction partners of a

plethora of cellular proteins, without consideration of their heterooligomeric context (for examples, see references in Peterson and Petty, 2010). Our study puts some of the previous literature in perspective, since the results suggest that septins are all assembled into heteromers according to "pairing rules" that coinciding with the previously defined sequence-homology subgroups. The data support that tissue-specific differences in septin composition reflect diversity within subgroups, and that all cell types express at least one representative of each of the four subgroups (Cao *et al.*, 2007). It follows that the cellular content of SEPT7—the sole member of its subgroup—is likely to be diagnostic for the total septin content in diverse mammalian cell types. Moreover, as depicted in Figure 10, core heteromers arranged according to subgroups imply that only a minor fraction of all native heteromers are arranged as perfect palindromes with respect to individual septin subunits.

The SEPT6 subgroup includes all mammalian septins with a G-domain motif predicting lack of intrinsic GTPase activity, while septins belonging to the other three subgroups are GTPase active (Sirajuddin *et al.*, 2009). Interestingly, as evidenced by structural differences between GTP- and GDP-bound states of human SEPT2 and phenotypes of specific septin mutations in yeast, it appears that a mixed interface between GDP- and GTP-bound septins provides stability of the heteromer units. We noted that stable octameric heteromers of budding yeast, as well as the dimer of the SEPT2/6/7 trimer, are arranged with a mixed G-interface between GDP- and GTP-bound septins (Sirajuddin *et al.*, 2009). Our results are consistent with the lack of GTPase activity of SEPT6 subgroup septins dictating the position within heteromers. However, the SEPT3-subgroup is predictively GTPase active, thus indicating a GDP–GDP interface within the stable octameric unit irrespective of how the four subgroups are arranged (Figure 10). Hence, the SEPT3-subgroup member SEPT9 appears not to depend on a mixed G-interface for a stable interaction within the octameric heteromer. This would be analogous to the only two septin proteins of the invertebrate *C. elegans* (Unc-59 and Unc-61), which predictably form an intraheteromeric GDP–GDP interface within core heteromers (John *et al.*, 2007).

Septins in budding yeast are arranged as octameric heteromers that polymerize via an NC-mode of interacting units. Notably, subpopulations of SEPT9-containing octamers in human cells share the predicted arrangement of G- and NC-dimer interfaces and consequently also an NC-interface at ends. In addition, differential polymerization interfaces at ends was hinted at by single-particle analysis, which suggested a minor subpopulation of heptamers. Alternative splicing of SEPT9 and consequent isoforms with variable N- or C-termini may also result in heteromers that are not arranged as perfect palindromes. At least some of these potential variations at heteromer ends may have consequences for higher-order structures. As evaluated by a simple partitioning assay, all individual septins, including the $SEPT9^{75\ kDa}$ and $SEPT9^{40\ kDa}$ isoforms, behave similarly with respect to their partitioning between a soluble and particulate state (Figure 2). However, future ultrastructural analysis may reveal differential localization of hexamers and octamers within higher structures, which in turn could illuminate and possibly differentiate functional roles of heteromer subpopulations.

MATERIALS AND METHODS

DNA constructs, cell culture, and transfections

Transfection of K562 and Jurkat cells using inducible Epstein-Barr virus–based replicating shuttle vectors was performed essentially as described elsewhere (Gradin *et al.*, 1998; Holmfeldt *et al.*, 2007). For transfection of constructs encoding SEPT6-Flag and SEPT7-Flag, 6–16 µg of the indicated construct was mixed with empty vector up to a total quantity of 16 µg of DNA. Transfections with replicating shuttle vectors directing constitutive expression of shRNAs against septins were performed by mixing 2 µg of the indicated shRNA construct with empty vector up to a total quantity of 16 µg of DNA. SEPT2 and SEPT5 were codepleted by mixing 2 µg of each shRNA construct with 12 µg of empty vector. Hygromycin-resistant cell lines were selected over 5–6 d. Over this time period, the ratio of transfected DNA was maintained due to the stringent replication control of the shuttle vector. Details on pMEP and shRNA shuttle vector derivatives are given in the Supplemental Material.

Analysis of proteins and mRNA

Western blotting followed by detection using the ECL Detection System (GE Healthcare, Waukesha, WI) was performed using anti-SEPT2 (11397-1-AP; ProteinTech Group, Chicago, IL), anti-SEPT5 (C20 sc-16610; Santa Cruz Biotechnology, Santa Cruz, CA), anti-SEPT6 (H60 sc-20180; Santa Cruz Biotechnology), anti-SEPT7 (JP18991; IBL International, Hamburg, Germany), anti-SEPT9 (10769-1-AP; ProteinTech Group), anti-SEPT11 (a kind gift from Pascale Cossart, Pasteur Institute, Paris), anti-Op18 (Holmfeldt *et al.*, 2003), anti-vimentin (2Q1123 sc-73258; Santa Cruz Biotechnology), or anti-tubulin (B-5-1-2; Sigma-Aldrich, St. Louis, MO) antibodies and the appropriate secondary reagents. For quantification of mRNA, qRT-PCR was used as described (Sellin *et al.*, 2008). PCR reactions were performed in triplicate using primer pairs specific for SEPT1-SEPT12 and SEPT14 (RT2 qPCR Primer Assays; SABiosciences, Frederick, MD).

Determination of protein partitioning between soluble and insoluble states

The assembly state of cytoskeletal proteins under various buffer conditions was evaluated by an assay based on the release of soluble protomer units after cell permeabilization (Marklund *et al.*, 1996). Cells were gently resuspended in the presence of 0.2% saponin, 10 µg/ml leupeptin in either 80 mM PIPES (pH 6.9; Cytoskeleton), 2 mM $MgCl_2$, 4 mM ethylene glycol tetraacetic acid (EGTA; 1X PEM buffer), twofold-diluted PEM buffer (0.5X PEM), or fourfold-diluted PEM buffer (0.25X PEM). The insoluble fraction was isolated by centrifugation (0.5 min, 2000 × *g*). Proteins in the pellet (i.e., the cell-associated insoluble fraction) and supernatant (i.e., released soluble cellular proteins) were resolved by SDS–PAGE and quantified by Western blotting as previously described (Marklund *et al.*, 1996).

Determination of hydrodynamic parameters of septins from crude cell lysates

HeLa, K562, or Jurkat cells were washed in phosphate-buffered saline, followed by permeabilization in PEM buffer (Sigma-Aldrich), 0.5% saponin, 10 µg/ml leupeptin on ice. Permeabilized cells were pelleted (5 min, 14,000 × *g*) and the supernatant, which contained >95% of all septins, was supplemented with 0.5 M NaCl to promote complete disassembly into protomer units. As saponin was used for cell permeabilization, the released cytosolic proteins were essentially devoid of membrane-derived lipids (Holmfeldt *et al.*, 2003), which minimized the risk that the hydrodynamic properties of septins are influenced by associated lipids. Hydrodynamic parameters were analyzed as previously described (Brannstrom *et al.*, 2009), with some modifications to account for the polymerization propensity and size range of septins. Accordingly, a phosphate buffer (10 mM, pH 7.5, 0.45 M NaCl) was used for both density-gradient centrifugation and gel-filtration chromatography. Sucrose gradients (10–30%) were run at 40,000 rpm for 16 h. Fractions were analyzed

by Western blotting using a panel of septin antibodies (see *Analysis of proteins and mRNA*), and signals were quantified by the Quantity One software (Bio-Rad, Hercules, CA). Molecular masses were calculated by combining gel-filtration and gradient sedimentation values in the equation described by Siegel and Monty (1966).

Immunoaffinity-based isolation of septin heteromers

K562 cells expressing FLAG-epitope–tagged septins were permeabilized as described in the previous section, and the soluble fraction was supplemented with 1% Triton X-100. Protein aggregates were removed by preclearing with control beads and centrifugation (10 min, 14,000 × *g*), and the supernatant was thereafter mixed with M2 anti-FLAG–coupled beads (Sigma-Aldrich) for 30 min at room temperature. Beads were collected and sedimented (1 min, 14 000 × *g*) through a wash gradient containing from the top 400 µl PEM, 0.1%Triton X-100; 400 µl PEM, 17% glycerol; and 400 µl PEM, 17% glycerol, 27% sucrose. Bound and unbound material was boiled in SDS sample buffer and analyzed by Western blotting. For elution of native septin heteromers, M2 beads were extensively washed and incubated at room temperature in PEM, 4 mM EGTA, 1 mM GTP, 5 µg/ml leupeptin supplemented with 100 µg/ml FLAG peptide. Elutes were supplemented with 0.30 M NaCl to ensure complete disassembly into heteromer units.

Electron microscopy visualization of purified septin heteromers

Purified septin heteromers were adsorbed for 2 min onto glow-discharged, carbon-coated copper grids. The samples were stained in 0.8% uranyl formate (3 drops of 50 µl for 10 s each), blotted, and air-dried. Sample examination was performed on a Philips CM120 transmission electron microscope (Karolinska Institute) operating at 100 kV. Septin heteromers were imaged at 110,000× magnification with approximately 1-µm defocus. Digital images were recorded using a MegaView III CCD camera (1376 × 1032 pixels) and analySIS software (Olympus Soft Imaging Solutions, Münster, Germany). Calibration with catalase crystals (S124; Agra Scientific, Stanstead, UK) resulted in a pixel size of 0.63 nm at this magnification.

ACKNOWLEDGMENTS

This work was supported by the Swedish Research Council. L.S. was supported by an EMBO long-term fellowship. Special thanks to Ian G. Macara and Pascale Cossart for generously providing cDNA and antibody reagents and to Sergej Masich and Bertil Daneholt for assistance with electron microscopy. We are also grateful for the advice on analysis of length distributions provided by Benoni Edin, Umeå University.

REFERENCES

Bertin A, McMurray MA, Grob P, Park SS, Garcia G III, Patanwala I, Ng HL, Alber T, Thorner J, Nogales E (2008). *Saccharomyces cerevisiae* septins: supramolecular organization of heterooligomers and the mechanism of filament assembly. Proc Natl Acad Sci USA 105, 8274–8279.

Brannstrom K, Sellin ME, Holmfeldt P, Brattsand M, Gullberg M (2009). The *Schistosoma mansoni* protein Sm16/SmSLP/SmSPO-1 assembles into a nine-subunit oligomer with potential to inhibit Toll-like receptor signaling. Infect Immun 77, 1144–1154.

Cao L, Ding X, Yu W, Yang X, Shen S, Yu L (2007). Phylogenetic and evolutionary analysis of the septin protein family in metazoan. FEBS Lett 581, 5526–5532.

Caudron F, Barral Y (2009). Septins and the lateral compartmentalization of eukaryotic membranes. Dev Cell 16, 493–506.

Estey MP, Di Ciano-Oliveira C, Froese CD, Bejide MT, Trimble WS (2010). Distinct roles of septins in cytokinesis: SEPT9 mediates midbody abscission. J Cell Biol 191, 741–749.

Field CM, al-Awar O, Rosenblatt J, Wong ML, Alberts B, Mitchison TJ (1996). A purified *Drosophila* septin complex forms filaments and exhibits GTPase activity. J Cell Biol 133, 605–616.

Gradin HM, Larsson N, Marklund U, Gullberg M (1998). Regulation of microtubule dynamics by extracellular signals: cAMP-dependent protein kinase switches off the activity of oncoprotein 18 in intact cells. J Cell Biol 140, 131–141.

Hall PA, Jung K, Hillan KJ, Russell SE (2005). Expression profiling the human septin gene family. J Pathol 206, 269–278.

Holmfeldt P, Brannstrom K, Stenmark S, Gullberg M (2003). Deciphering the cellular functions of the Op18/stathmin family of microtubule-regulators by plasma membrane-targeted localization. Mol Biol Cell 14, 3716–3729.

Holmfeldt P, Stenmark S, Gullberg M (2007). Interphase-specific phosphorylation-mediated regulation of tubulin dimer partitioning in human cells. Mol Biol Cell 18, 1909–1917.

Hu Q, Milenkovic L, Jin H, Scott MP, Nachury MV, Spiliotis ET, Nelson WJ (2010). A septin diffusion barrier at the base of the primary cilium maintains ciliary membrane protein distribution. Science 329, 436–439.

Huang YW, Surka MC, Reynaud D, Pace-Asciak C, Trimble WS (2006). GTP binding and hydrolysis kinetics of human septin 2. FEBS J 273, 3248–3260.

John CM *et al*. (2007). The *Caenorhabditis elegans* septin complex is nonpolar. EMBO J 26, 3296–3307.

Kim SK *et al*. (2010). Planar cell polarity acts through septins to control collective cell movement and ciliogenesis. Science 329, 1337–1340.

Kinoshita M (2003a). Assembly of mammalian septins. J Biochem 134, 491–496.

Kinoshita M (2003b). The septins. Genome Biol 4, 236.

Kinoshita M, Field CM, Coughlin ML, Straight AF, Mitchison TJ (2002). Self- and actin-templated assembly of mammalian septins. Dev Cell 3, 791–802.

Kremer BE, Haystead T, Macara IG (2005). Mammalian septins regulate microtubule stability through interaction with the microtubule-binding protein MAP4. Mol Biol Cell 16, 4648–4659.

Low C, Macara IG (2006). Structural analysis of septin 2, 6, and 7 complexes. J Biol Chem 281, 30697–30706.

Lukoyanova N, Baldwin SA, Trinick J (2008). 3D reconstruction of mammalian septin filaments. J Mol Biol 376, 1–7.

Marklund U, Larsson N, Gradin HM, Brattsand G, Gullberg M (1996). Oncoprotein 18 is a phosphorylation-responsive regulator of microtubule dynamics. EMBO J 15, 5290–5298.

Mendoza M, Hyman AA, Glotzer M (2002). GTP binding induces filament assembly of a recombinant septin. Curr Biol 12, 1858–1863.

Oh Y, Bi E (2011). Septin structure and function in yeast and beyond. Trends Cell Biol 21, 141–148.

Pan F, Malmberg RL, Momany M (2007). Analysis of septins across kingdoms reveals orthology and new motifs. BMC Evol Biol 7, 103.

Peterson EA, Petty EM (2010). Conquering the complex world of human septins: implications for health and disease. Clin Genet 77, 511–524.

Sellin ME, Holmfeldt P, Stenmark S, Gullberg M (2008). Global regulation of the interphase microtubule system by abundantly expressed Op18/stathmin. Mol Biol Cell 19, 2897–2906.

Sheffield PJ, Oliver CJ, Kremer BE, Sheng S, Shao Z, Macara IG (2003). Borg/septin interactions and the assembly of mammalian septin heterodimers, trimers, and filaments. J Biol Chem 278, 3483–3488.

Siegel LM, Monty KJ (1966). Determination of molecular weights and frictional ratios of proteins in impure systems by use of gel filtration and density gradient centrifugation. Application to crude preparations of sulfite and hydroxylamine reductases. Biochim Biophys Acta 112, 346–362.

Sirajuddin M, Farkasovsky M, Hauer F, Kuhlmann D, Macara IG, Weyand M, Stark H, Wittinghofer A (2007). Structural insight into filament formation by mammalian septins. Nature 449, 311–315.

Sirajuddin M, Farkasovsky M, Zent E, Wittinghofer A (2009). GTP-induced conformational changes in septins and implications for function. Proc Natl Acad Sci USA 106, 16592–16597.

Tooley AJ, Gilden J, Jacobelli J, Beemiller P, Trimble WS, Kinoshita M, Krummel MF (2009). Amoeboid T lymphocytes require the septin cytoskeleton for cortical integrity and persistent motility. Nat Cell Biol 11, 17–26.

Weirich CS, Erzberger JP, Barral Y (2008). The septin family of GTPases: architecture and dynamics. Nat Rev Mol Cell Biol 9, 478–489.